Supplementary information

Global biogenic isoprene emissions 2013-2020 inferred from satellite isoprene observations

Hui Li[1,2#], Philippe Ciais[1], Pramod Kumar[1], Didier A. Hauglustaine[1], Frédéric Chevallier[1], Grégoire Broquet[1], Dylan B. Millet[3], Kelley C. Wells[3], Jinghui Lian[1,4], Bo Zheng[2,5]

[1]Laboratoire des Sciences du Climat et de l'Environnement, LSCE/IPSL, CEA-CNRS-UVSQ, Université Paris-Saclay, F-91191 Gif-sur-Yvette, France.
[2]Shenzhen Key Laboratory of Ecological Remediation and Carbon Sequestration, Institute of Environment and Ecology, Tsinghua Shenzhen International Graduate School, Tsinghua University, Shenzhen 518055, China.
[3]University of Minnesota, St. Paul, MN 55108, USA.
[4]Origins.earth, SUEZ Group, Immeuble Altiplano, 4 Place de la Pyramide, 92800 Puteaux, France
[5]State Environmental Protection Key Laboratory of Sources and Control of Air Pollution Complex, Beijing 100084, China.

Correspondence to: Hui Li (hui.li@lsce.ipsl.fr)

This file includes:

- Figures S1 to S25
- Tables S1-S3

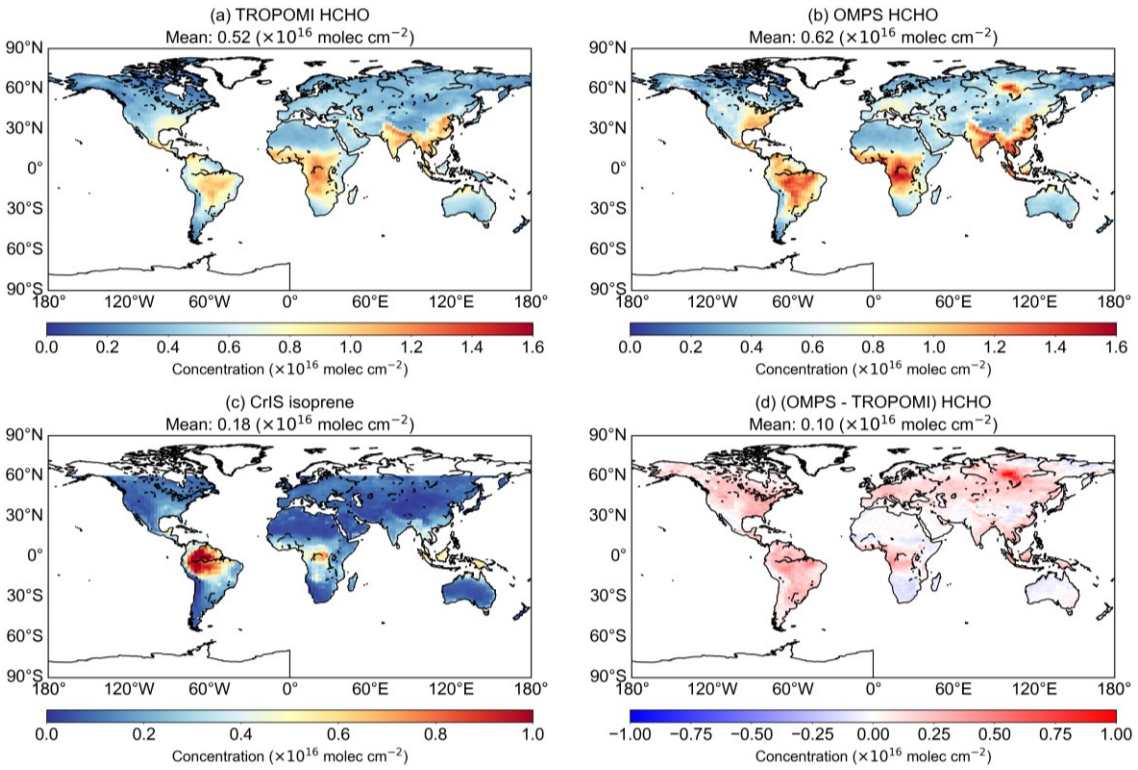

Figure S1. The global distribution of annual average HCHO and isoprene concentration in 2019. (a) and (b) present the HCHO concentration from TROPOMI and OMPS. (c) shows the isoprene concentration from CrIS. (d) shows the difference between OMPS and TROPOMI HCHO concentration.

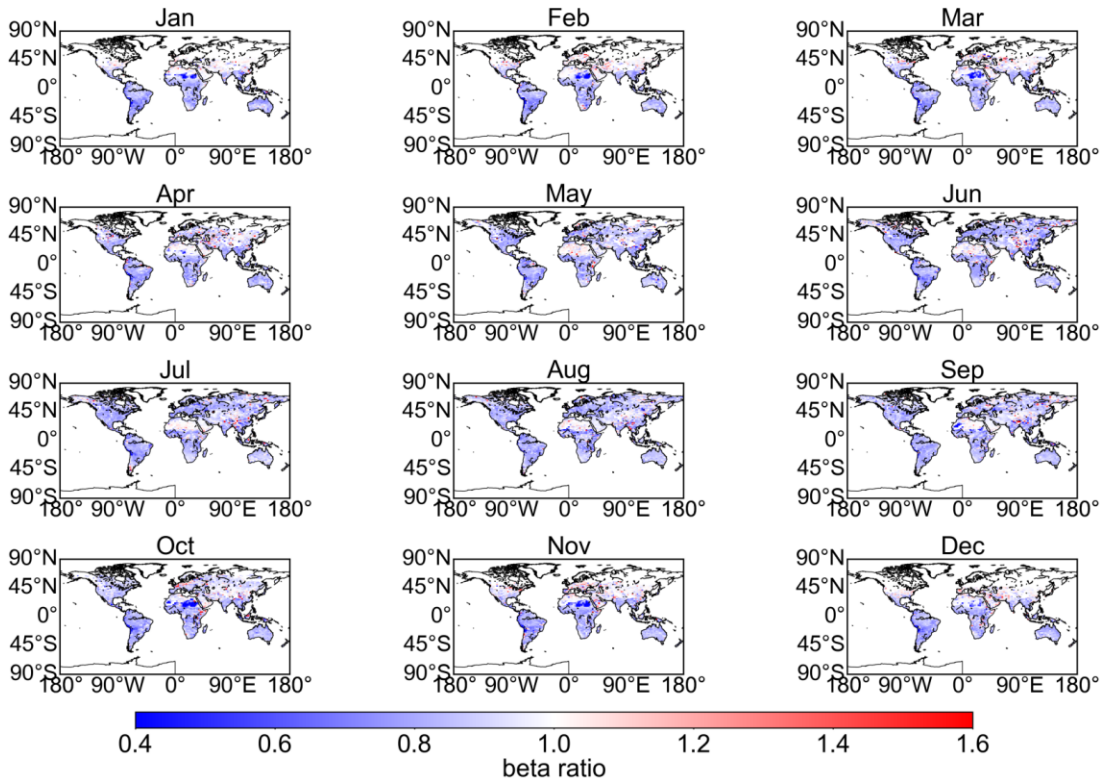

Figure S2. The distribution of ($\beta_{+25\%}/\beta_{-40\%}$) ratio in 2019.

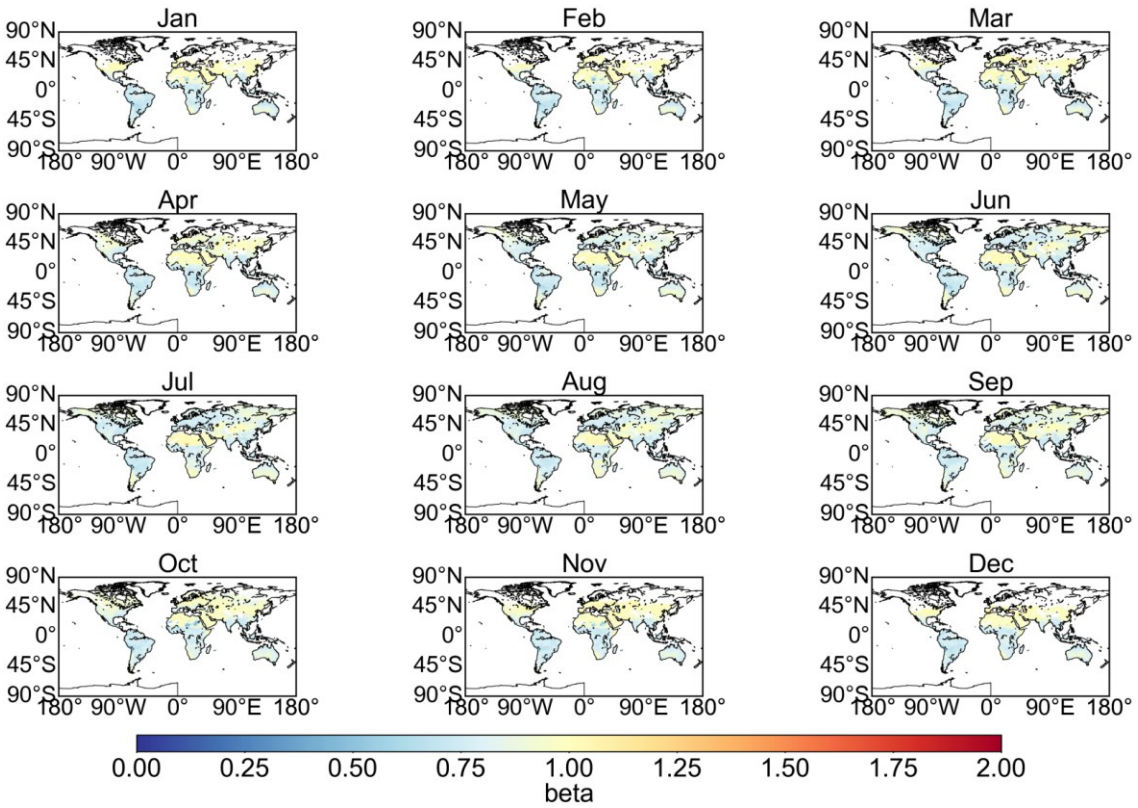

Figure S3. An example of monthly β distribution in 2019.

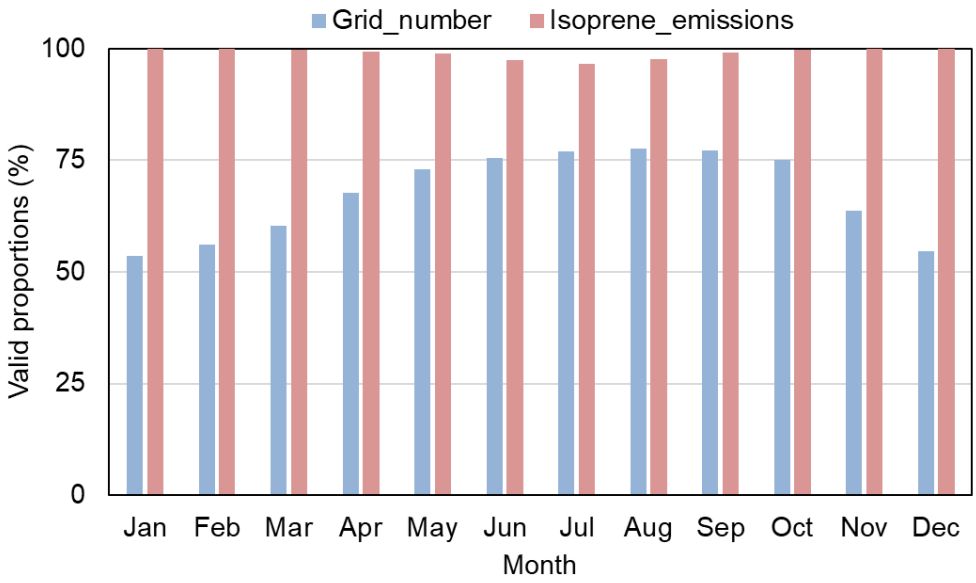

Figure S4. Proportions of grids with updated emissions, including the grid number proportions and emission proportions. We here use prior maps to calculate the proportions.

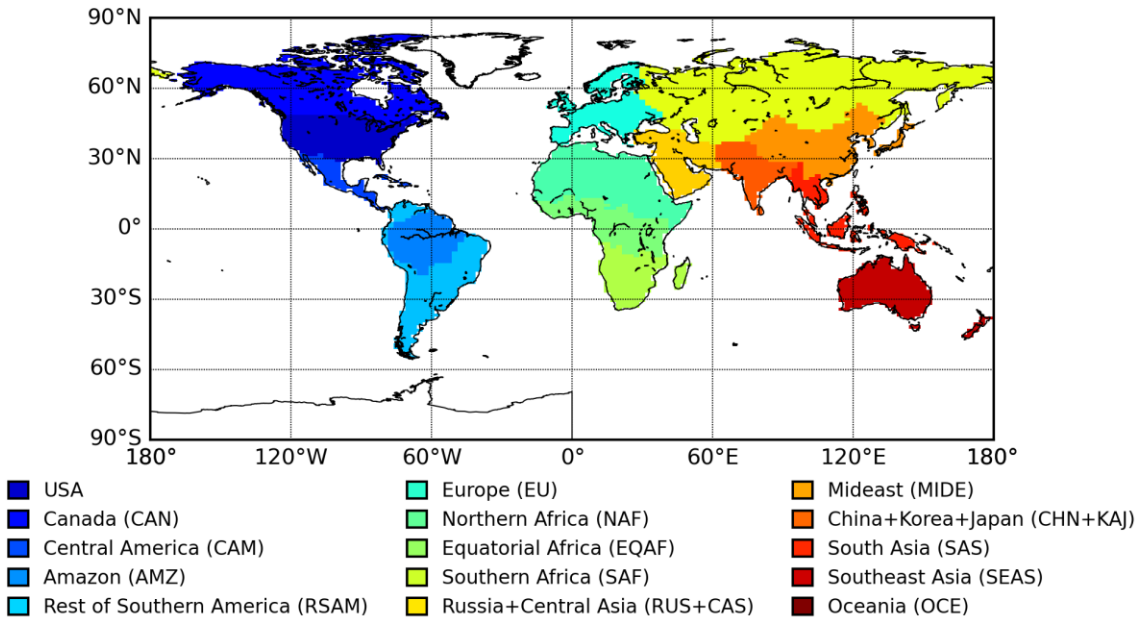

Figure S5. The 15-region classification in this study.

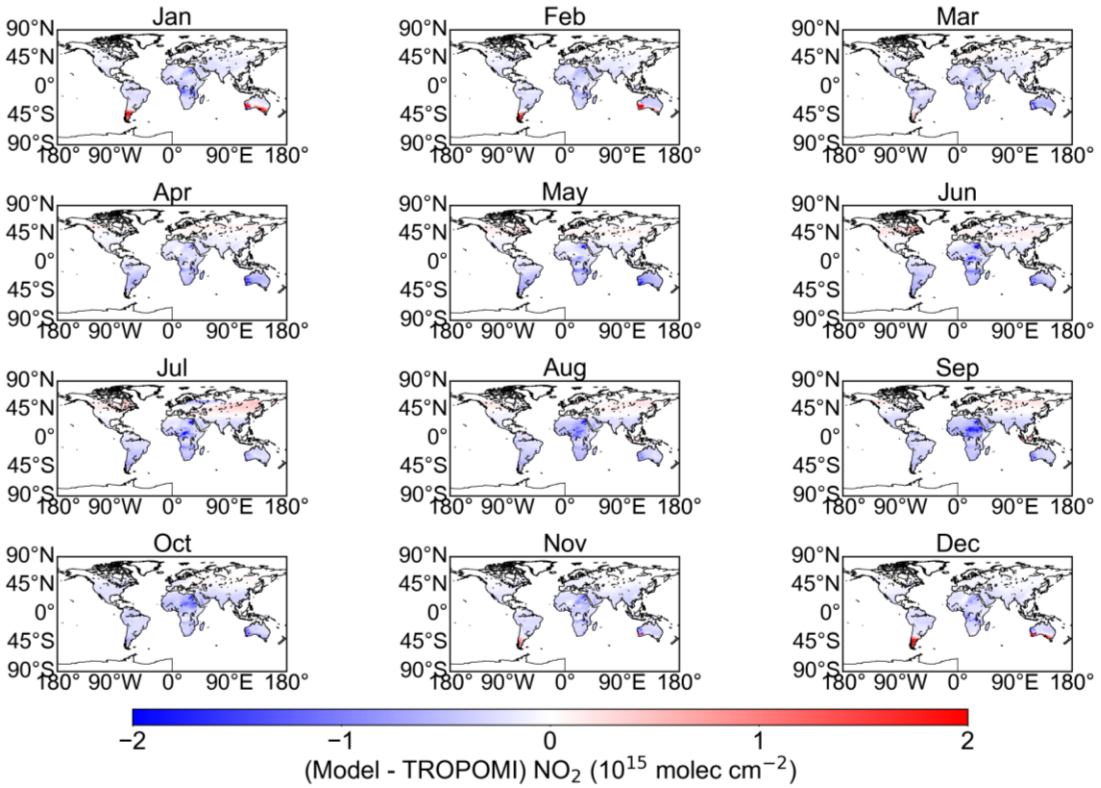

47

48 **Figure S6**. Comparison of LMDZ-INCA simulated NO_2 with TROPOMI observed NO_2 column
49 concentration in 2019. Here the modeled NO_2 concentration has been resampled at TROPOMI overpass
50 time and recalculated as model equivalence, the same as HCHO process.

51

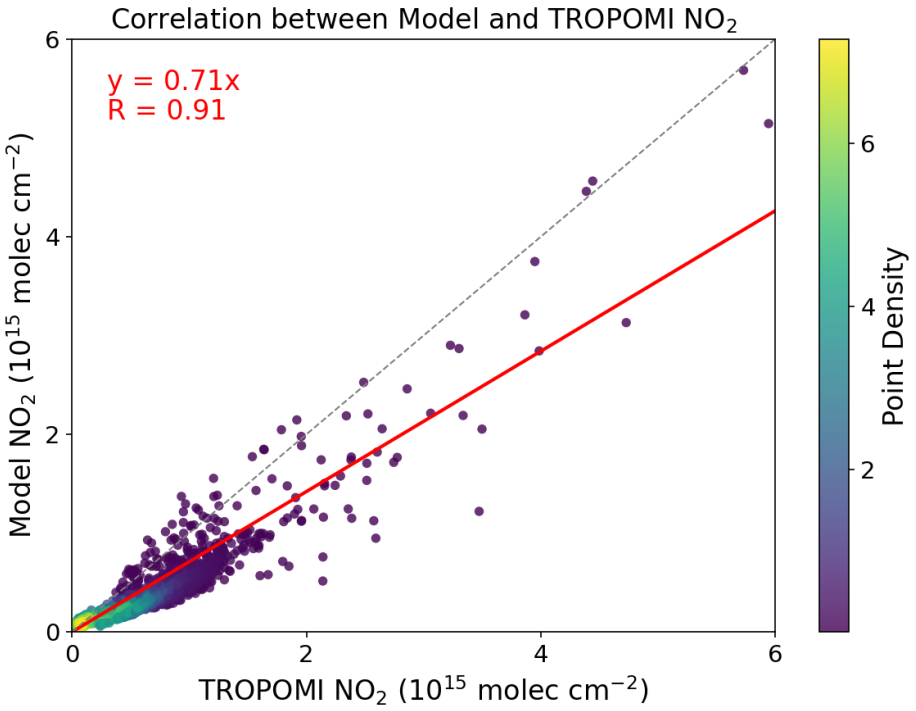

Figure S7. Correlation of LMDZ-INCA simulated NO_2 with TROPOMI observed NO_2 column concentration, colored by the grid density.

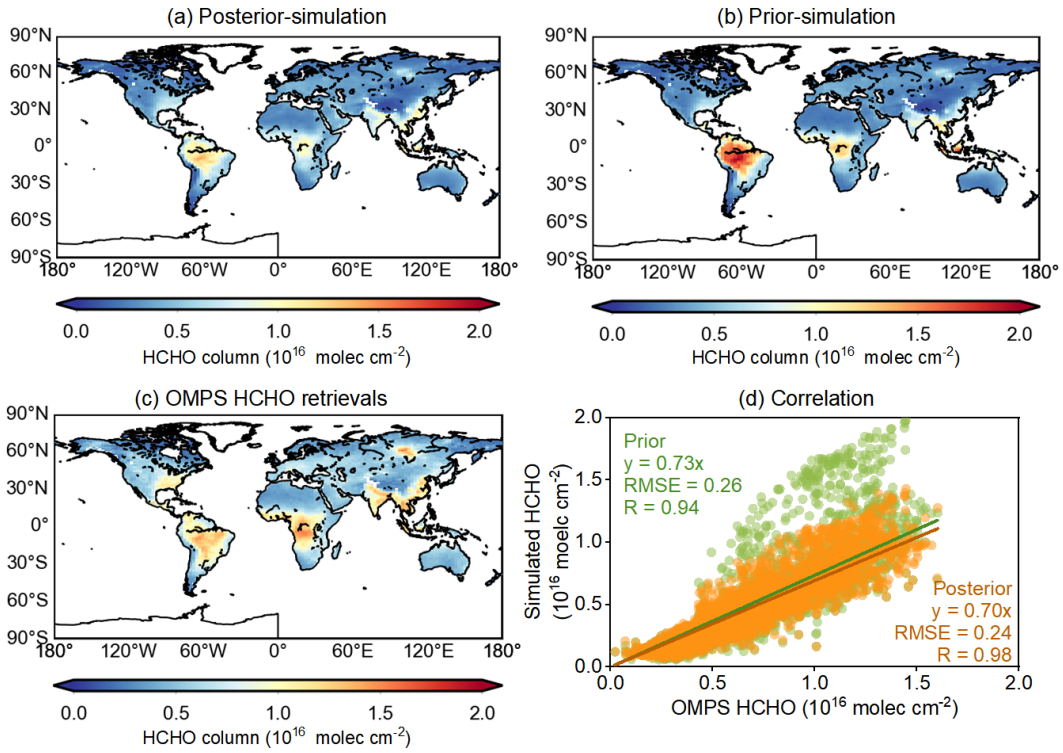

Figure S8. Comparison of simulated HCHO with OMPS observed HCHO column concentration.

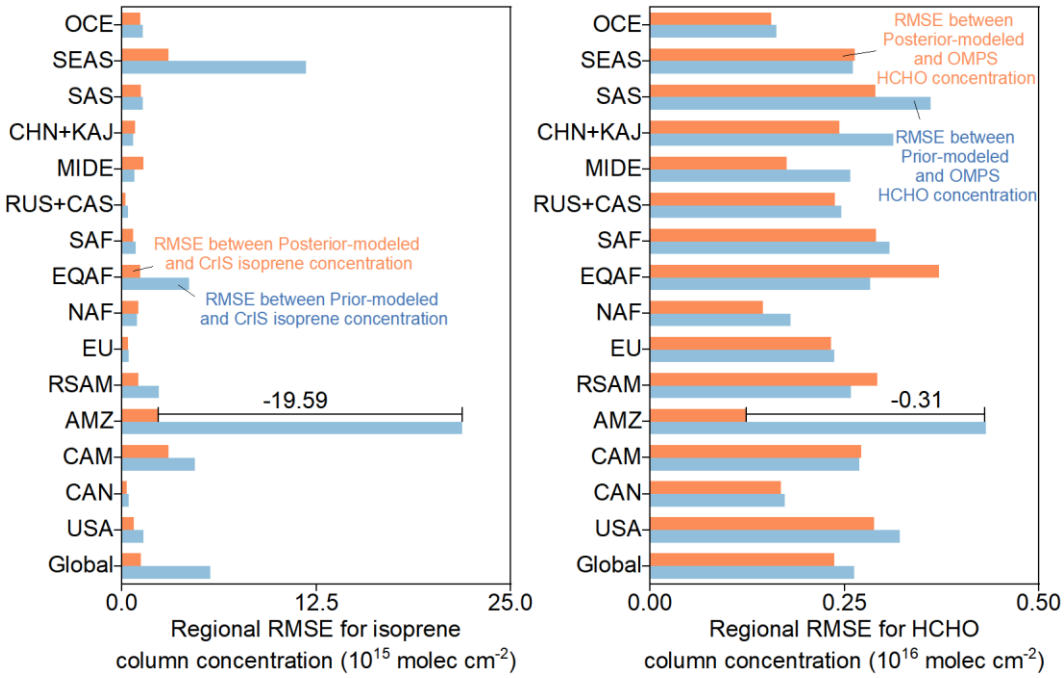

Figure S9. Global and regional Root Mean Squared Error (RMSE) for isoprene (left panel) and HCHO (right panel) column concentrations.

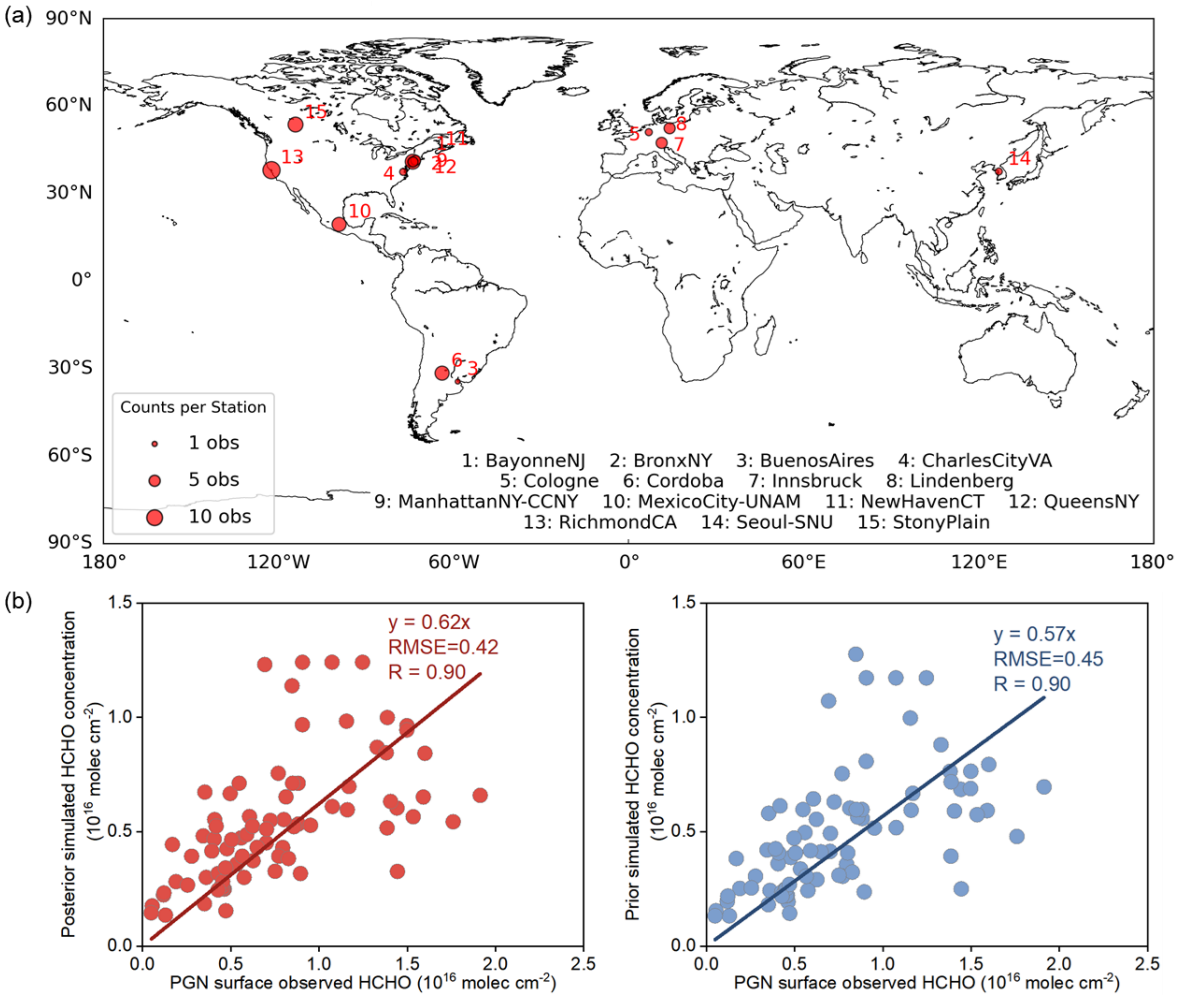

Figure S10. The comparison of HCHO column concentration between simulation and PGN surface observation. (a) shows the distribution of PGN stations used in this study, which provided official data for 2019 and are located between 60°S and 60°N. (b) compares the correlation between posterior simulated, prior simulated and PGN observed HCHO column concentrations. PGN data are acquired from https://www.pandonia-global-network.org/.

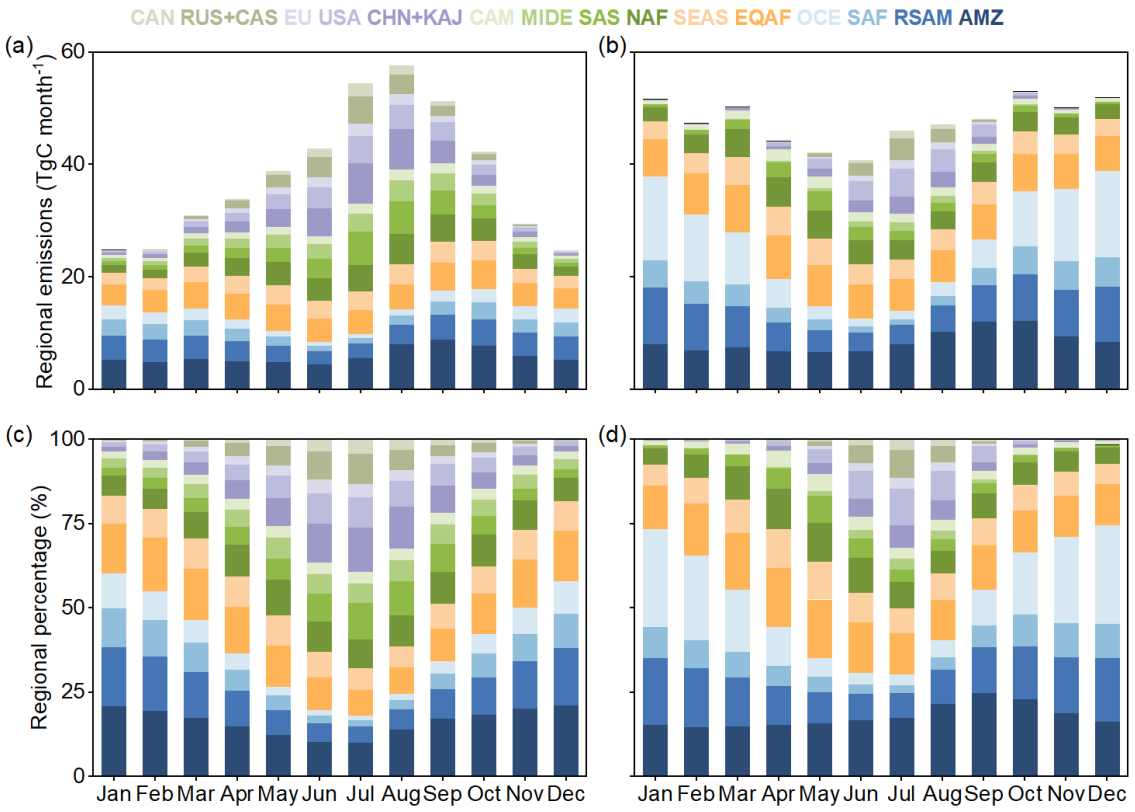

Figure S11. The comparison of regional monthly emissions between posteriors and MEGAN-MACC. (a) and (c) are the monthly absolute isoprene emissions and proportions to global totals for posteriors. (b) and (d) are the same for MEGAN-MACC inventory.

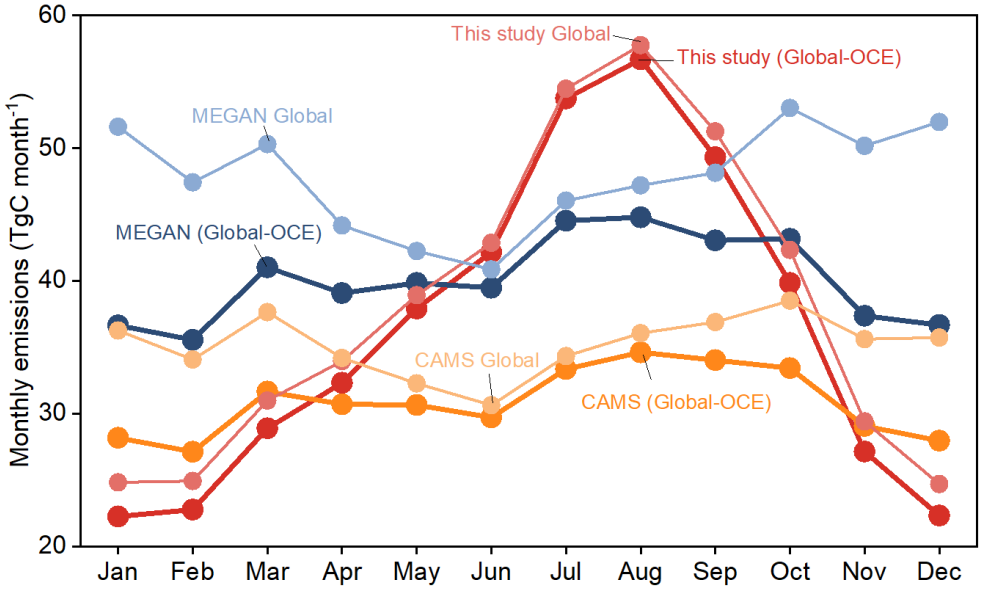

Figure S12. The comparison of seasonal patterns between posterior and inventories with and without Oceania (OCE) region.

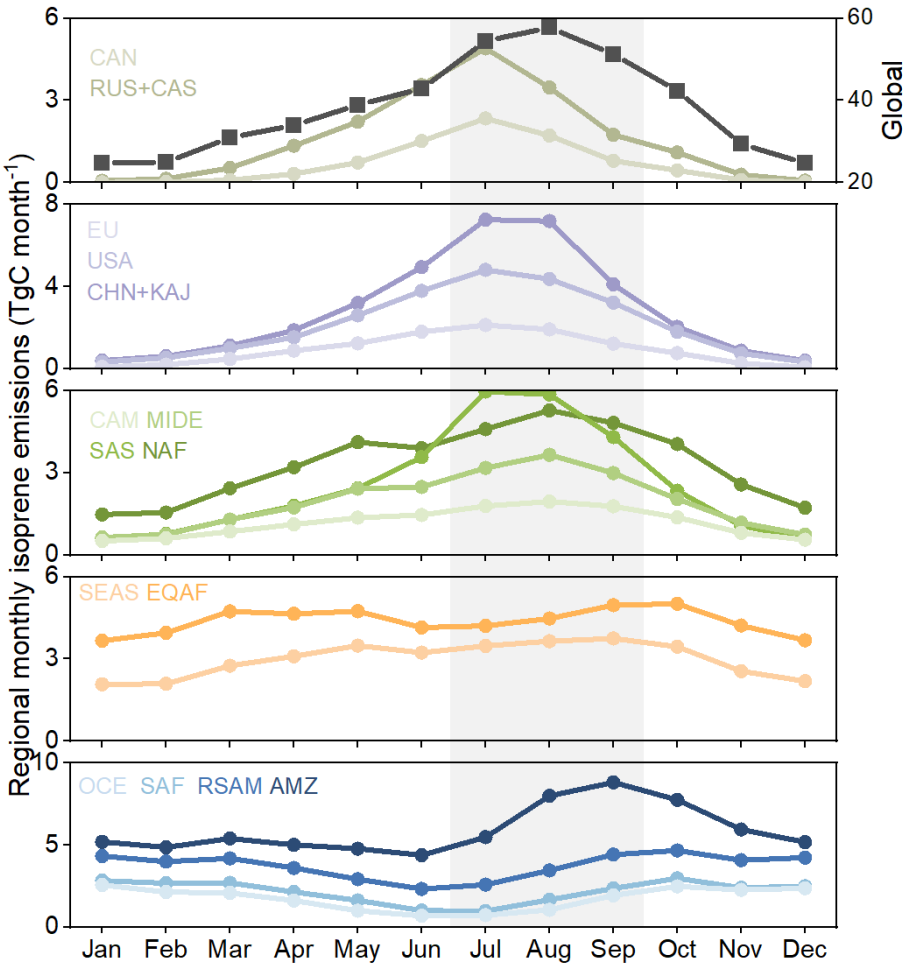

Figure S13. Monthly pattern of regional isoprene emissions averaged from 2013 to 2020.

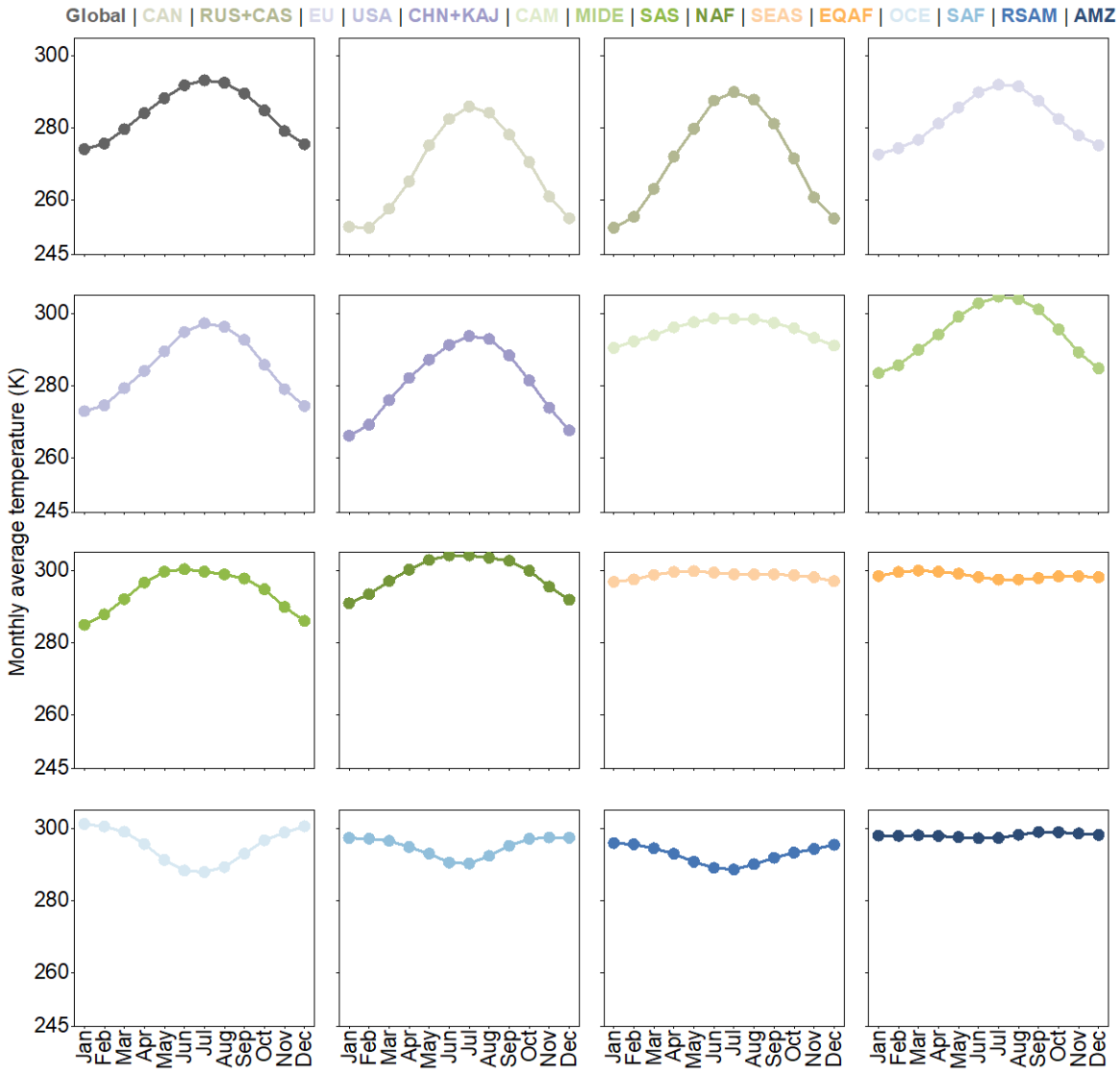

Figure S14. Global and regional monthly temperature fluctuation, with color referring regions. To highlight the fluctuation, the y-axis range are set to be the same in all panels. Data are acquired from ERA5 (https://cds.climate.copernicus.eu/datasets/reanalysis-era5-single-levels?tab=overview).

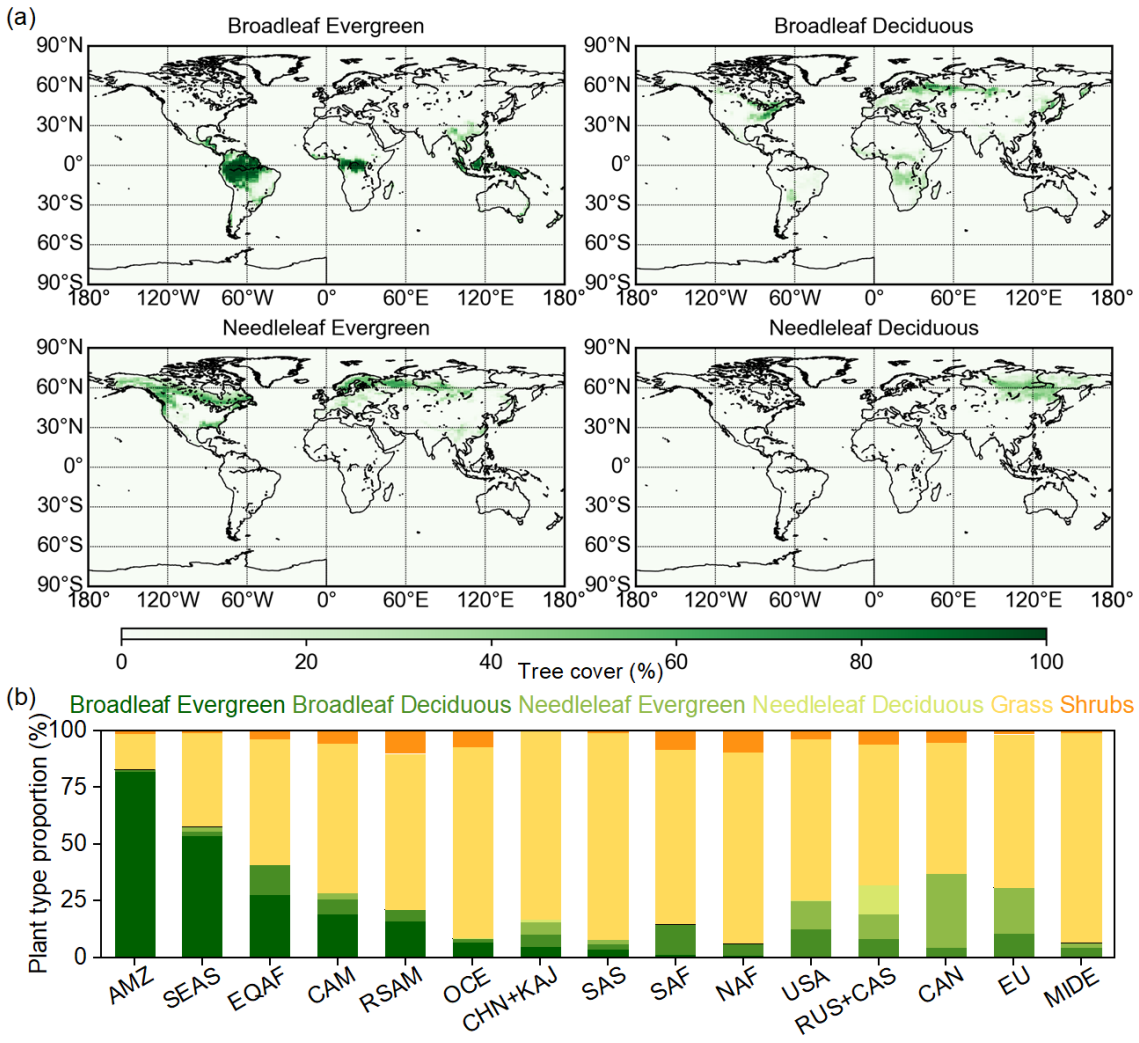

87

88 **Figure S15**. Distribution of plant type averaged from 2013 to 2020. (a) shows the four tress types
89 distribution and (b) presents the percentage of all plant type in each region. Data are acquired from ESA
90 Land Cover Climate Change Initiative (Land_Cover_cci): Global Plant Functional Types (PFT) Dataset,
91 v2.0.8 (Li et al., 2018).

92

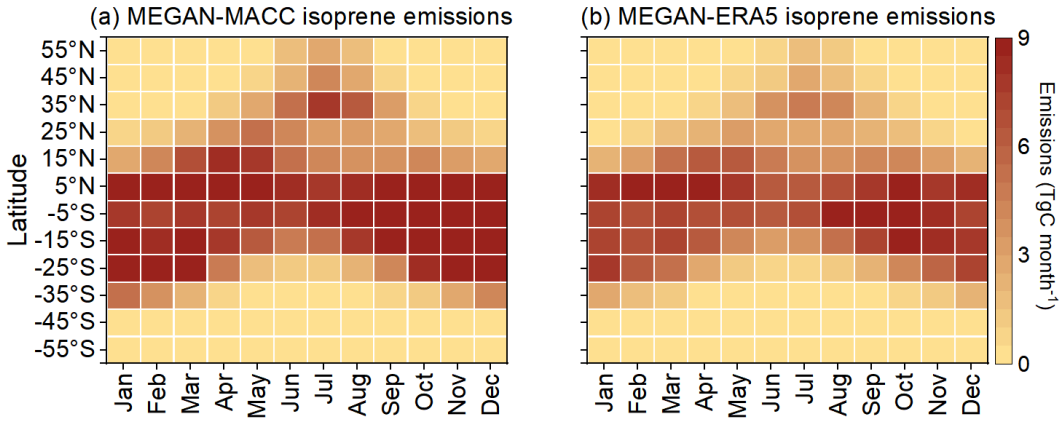

93

94 **Figure S16**. Monthly distributions of MEGAN-MACC and MEGAN-ERA5 by every 10° latitude band,
95 respectively.

96

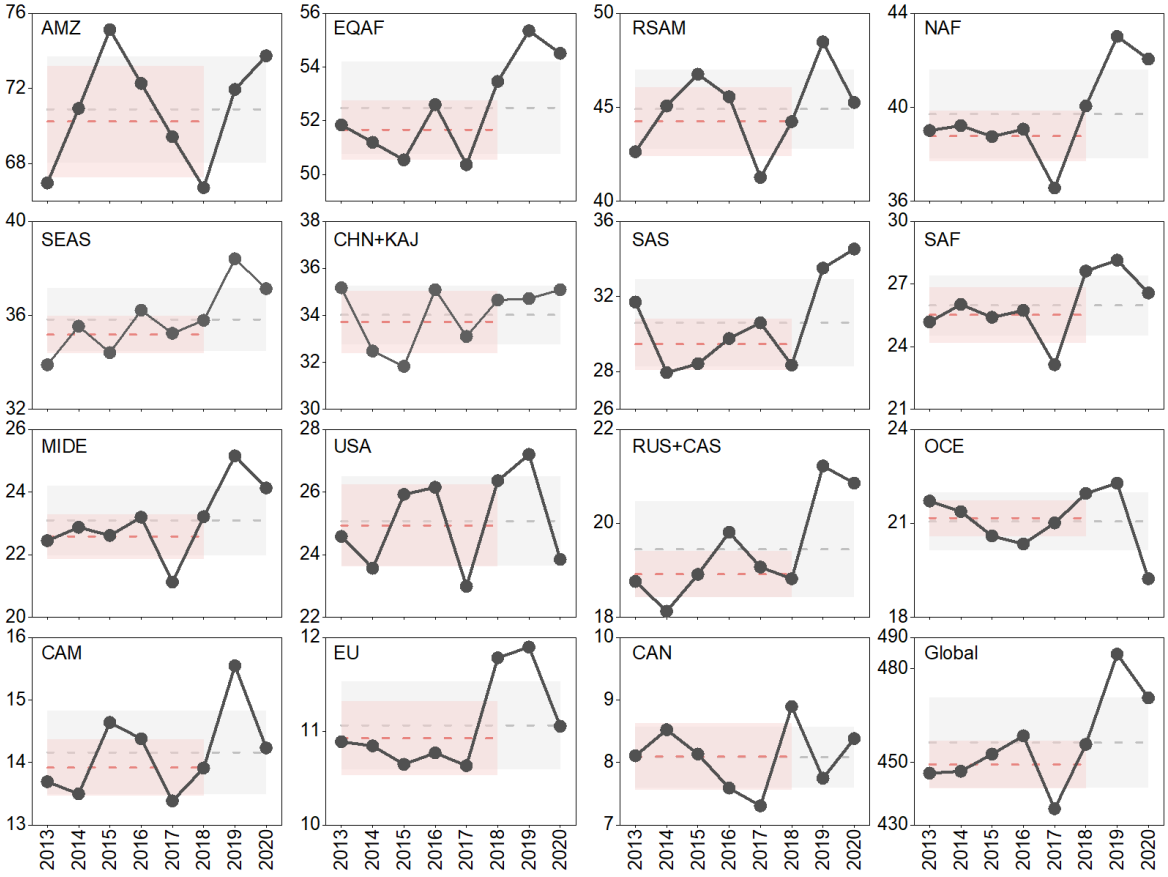

Figure S17. Annual global and regional isoprene emissions (TgC yr^{-1}) from 2013 to 2020. The gray dashed line is the annual average isoprene emissions from 2013 to 2020, and the gray shadow indicate corresponding one standard deviation (1σ). The red dashed line is the annual average isoprene emissions from 2013 to 2018, and the red shadow indicate corresponding one standard deviation (1σ).

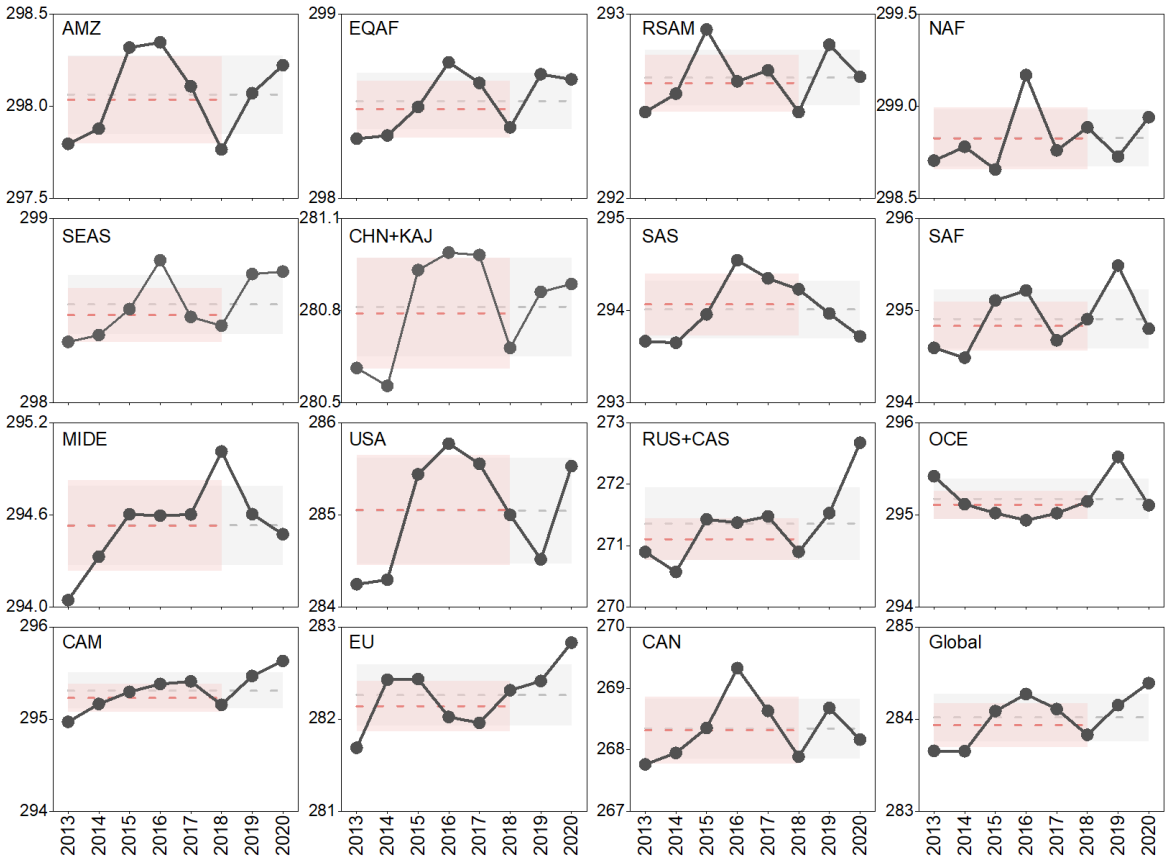

Figure S18. Regional and global annual average temperature (K) over land area from 2013 to 2020. The gray dashed line is the annual average temperature from 2013 to 2020, and the gray shadow indicate corresponding one standard deviation (1σ). The red dashed line is the annual average temperature from 2013 to 2018, and the red shadow indicate corresponding one standard deviation (1σ).

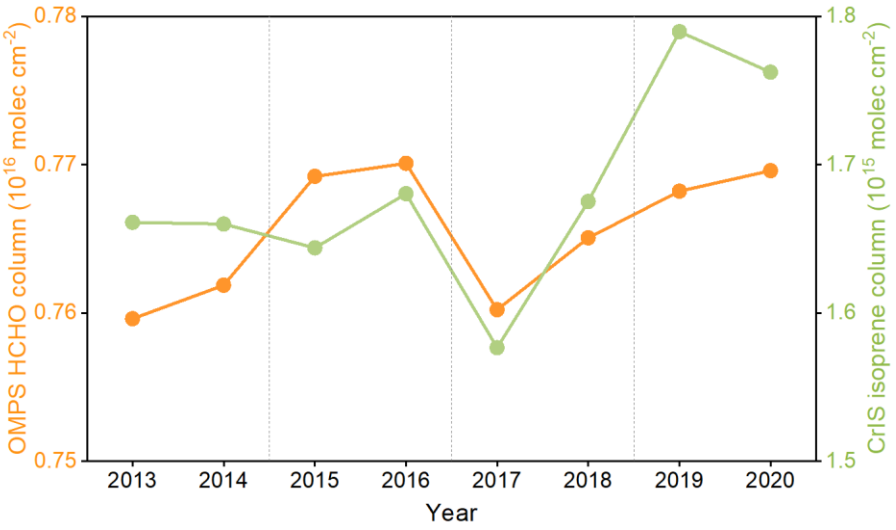

Figure S19. Annual average OMPS HCHO concentration and CrIS isoprene concentration from 2013 to 2020.

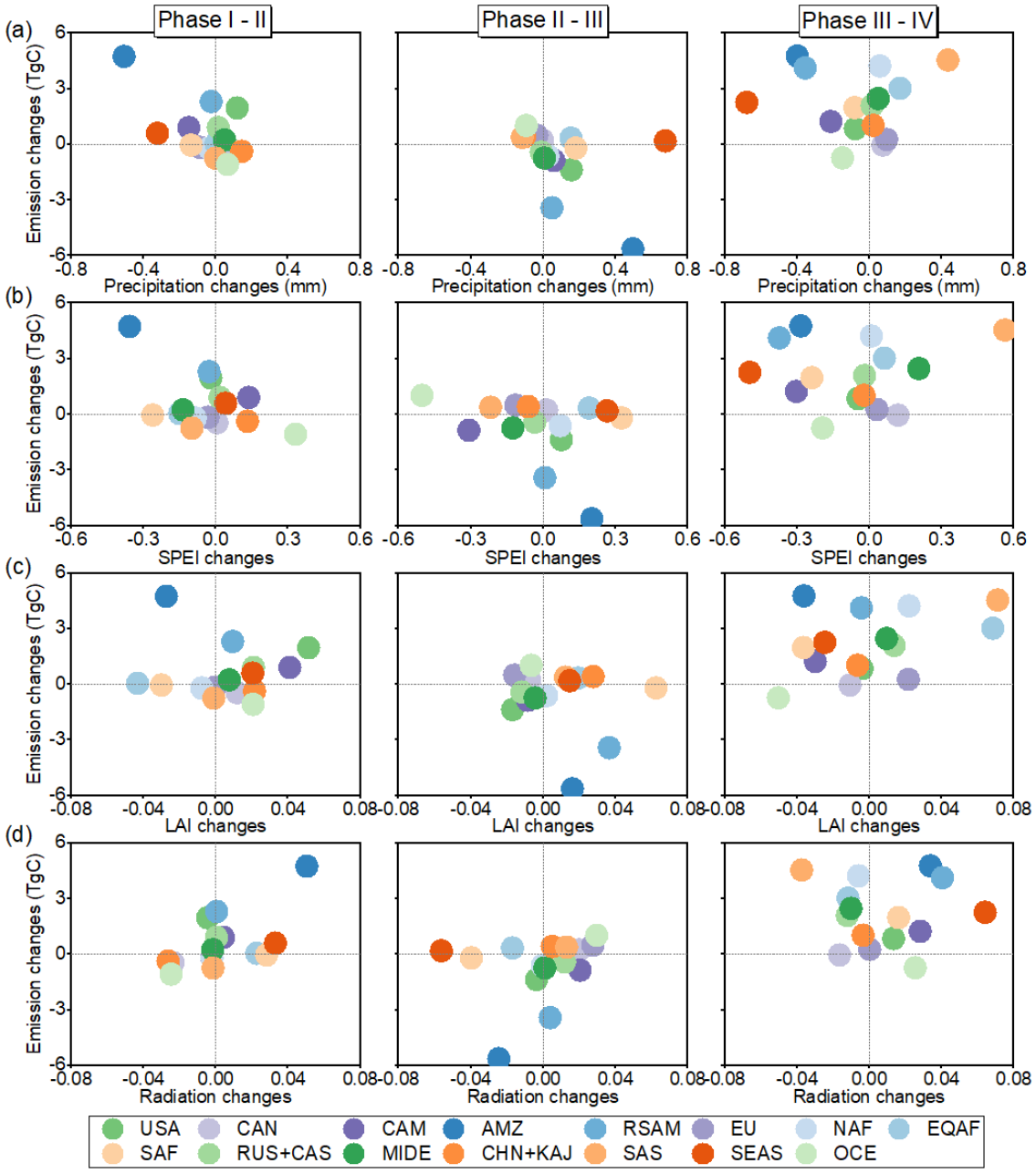

Figure S20. Correlation between the regional isoprene emission changes and (a) precipitation changes (mm), (b) SPEI changes, (c) Leaf area index (LAI) changes, and (d) radiation (MJ m^{-2}) across four phases. SPEI data is from ECMWF (https://xds-preprod.ecmwf.int/datasets/derived-drought-historical-monthly?tab=overview). LAI is acquired from Pu et al. (2024).

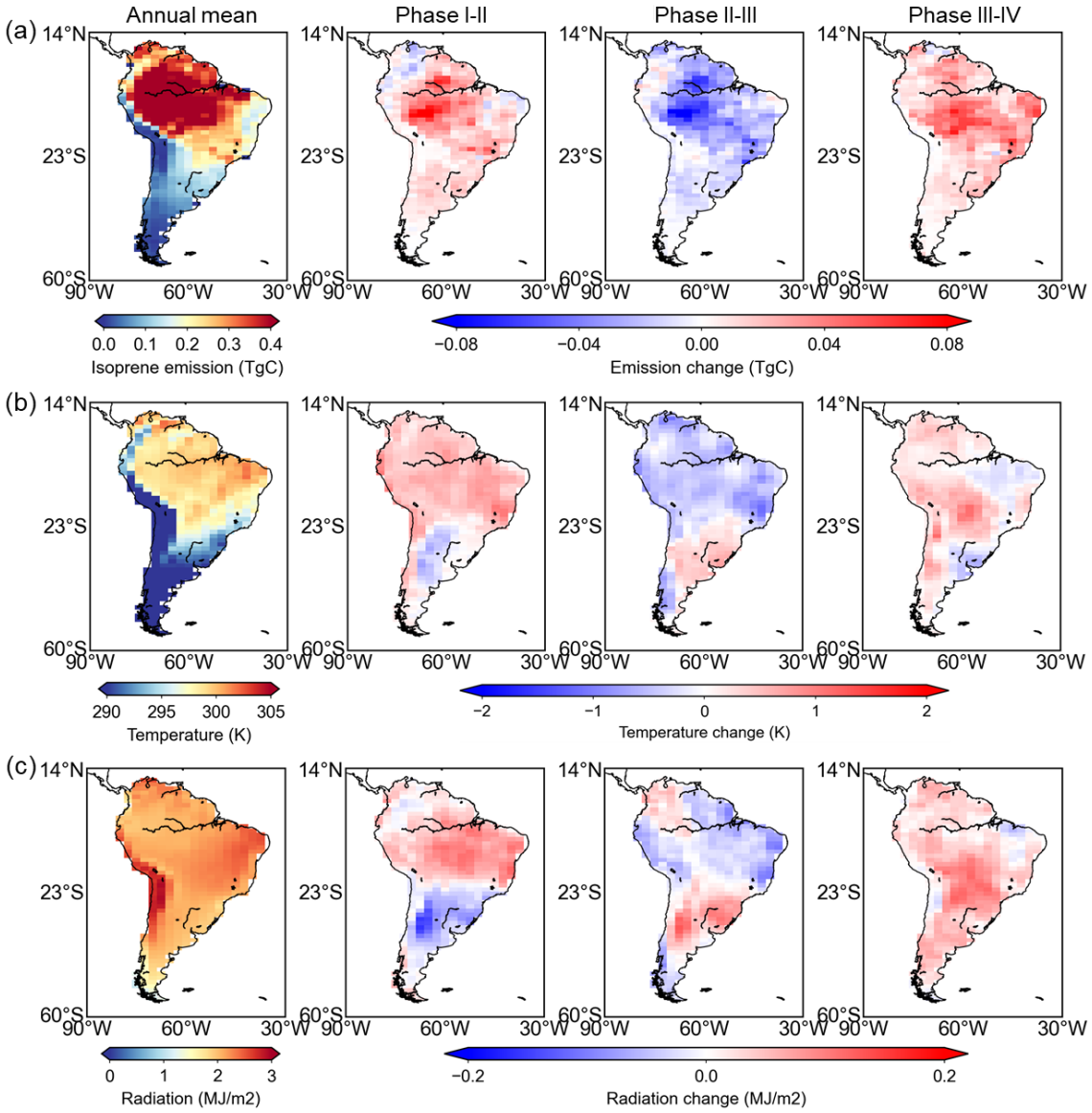

Figure S21. Regional annual mean and their changes across phases in Southern America (AMZ and RSAM) for (a) isoprene emissions, (b) temperature, and (c) radiation. The first column shows the annual mean, and the second to fourth columns correspond to the changes in regional values across phases.

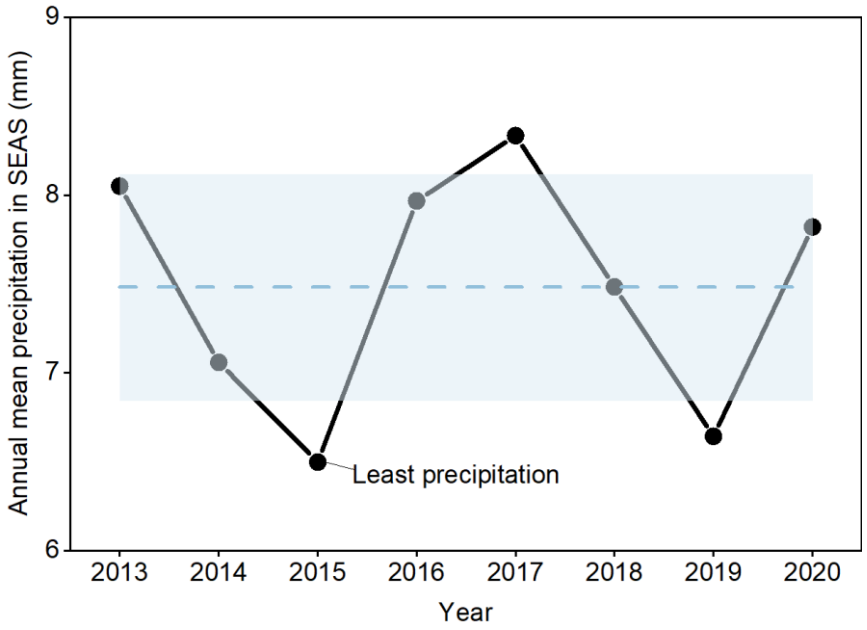

Figure S22. Annual average precipitation in SEAS from 2013 to 2020.

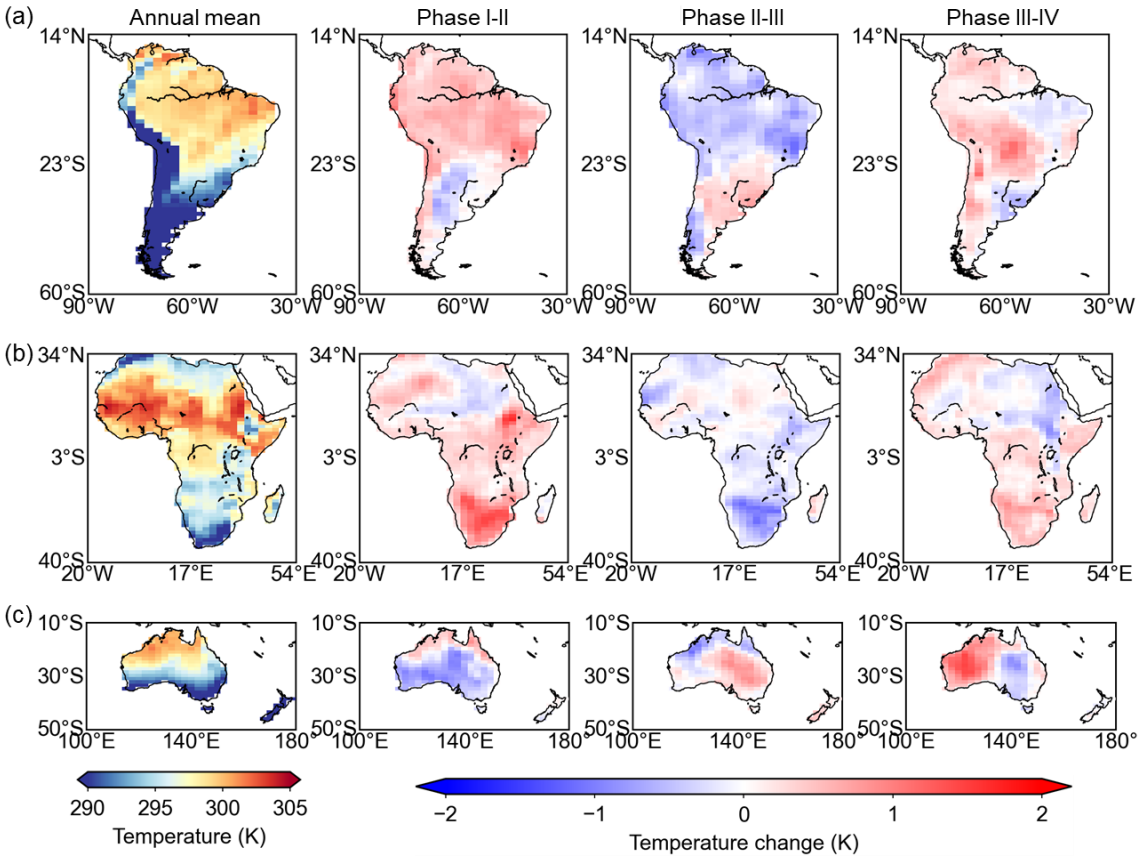

Figure S23. Regional annual average temperature and their changes across phases for (a) Southern America including AMZ and RSAM, (b) Africa including NAF, EQAF, and SAF, and (c) OCE. The first column shows the annual mean temperature for each region, and the second to fourth columns correspond to the changes in regional temperature across phases.

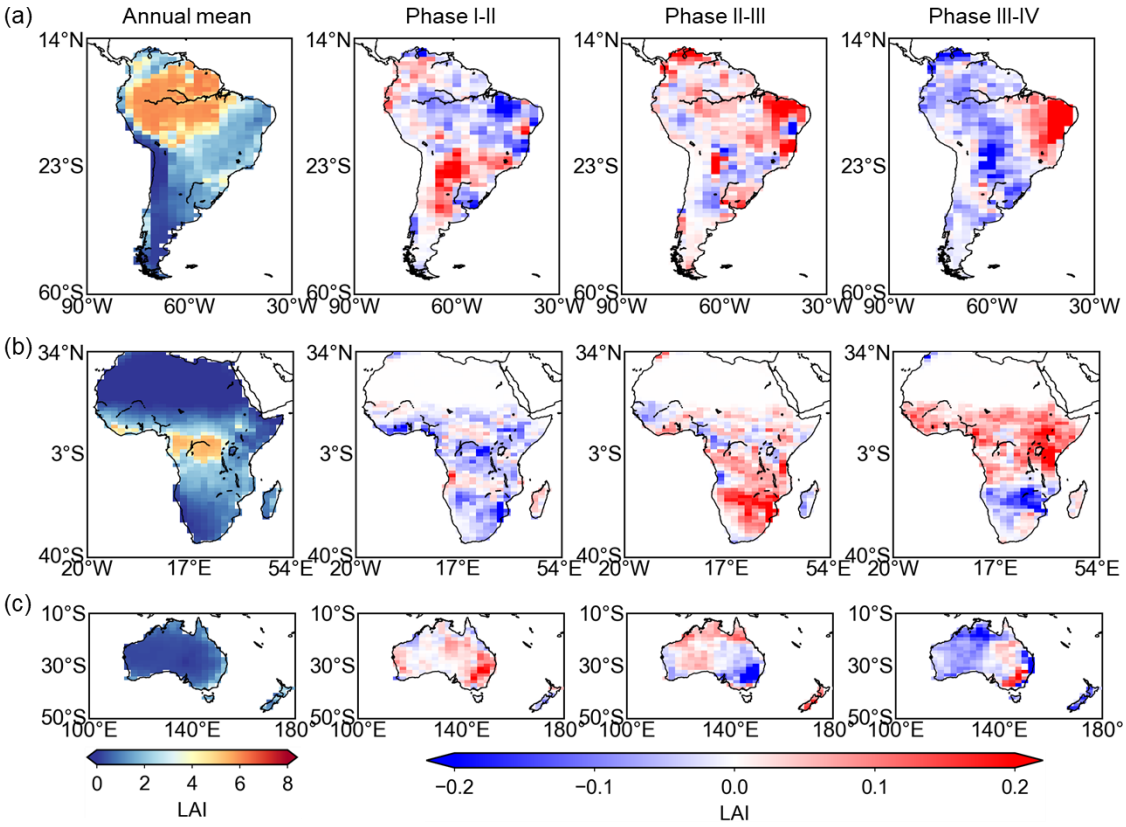

Figure S24. Regional annual average LAI and their changes across phases for (a) Southern America including AMZ and RSAM, (b) Africa including NAF, EQAF, and SAF, and (c) OCE. The first column shows the annual mean LAI for each region, and the second to fourth columns correspond to the changes in regional LAI across phases. LAI is from Pu et al. (2024).

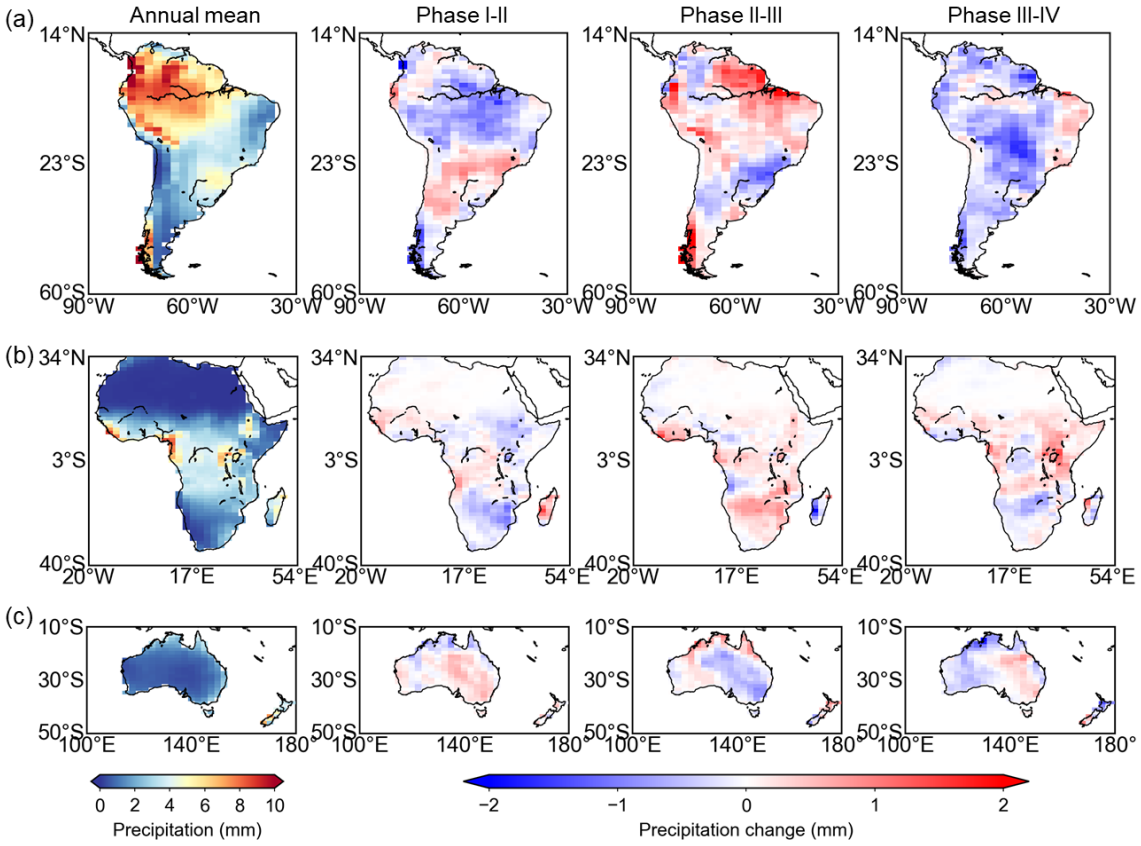

Figure S25. Regional annual average precipitation and their changes across phases for (a) Southern America including AMZ and RSAM, (b) Africa including NAF, EQAF, and SAF, and (c) OCE. The first column shows the annual mean precipitation for each region, and the second to fourth columns correspond to the changes in regional precipitation across phases.

Table S1. Correlation coefficient of monthly isoprene emissions and meteorological factors and LAI. Regional classification is seen in Fig. S5.

Correlation coefficient (R)	Temperature	LAI	Precipitation	Radiation	SPEI
AMZ (Amazon)	0.76	-	-0.69	0.82	-0.48
EQAF (Equatorial Africa)	-	0.72	0.65	-	-
RSAM (Rest of Southern America)	0.75	0.41	0.42	0.82	-0.25
NAF (Northern Africa)	0.92	0.88	0.90	0.69	0.26
SEAS (Southeast Asia)	0.79	0.73	0.57	-	-0.23
CHN+KAJ (China+Korea+Japan)	0.91	0.98	0.96	0.71	0.24
SAS (South Asia)	0.79	0.72	0.96	-	-
SAF (Southern Africa)	0.92	0.52	0.61	0.87	-
MIDE (Mideast)	0.95	0.74	-0.74	0.80	-
USA (the United States)	0.96	0.98	-	0.85	-
RUS+CAS (Russia+Central Asia)	0.93	0.98	0.92	0.82	-0.56
OCE (Oceania)	0.91	0.40	0.40	0.94	-
CAM (Central America)	0.93	0.84	0.80	0.65	-
EU (Europe)	0.96	0.97	-	0.90	-0.31
CAN (Canada)	0.90	0.98	0.81	0.70	
Global total	0.92	0.89	0.87	0.62	-0.43

*Insignificant correlations ($p>0.05$) are labeled with "-" in the table.

Table S2. Regional and global annual isoprene emissions from 2013 to 2020 (TgC yr^{-1}). Regional classification is seen in Fig. S5.

Isoprene (TgC yr^{-1})	2013	2014	2015	2016	2017	2018	2019	2020
AMZ	67	71	75	72	69	67	72	74
EQAF	52	51	51	53	50	53	55	55
RSAM	43	45	47	46	41	44	48	45
NAF	39	39	39	39	37	40	43	42
SEAS	34	36	34	36	35	36	38	37
CHN+KAJ	35	32	32	35	33	35	35	35
SAS	32	28	28	30	31	28	34	35
SAF	25	26	25	26	23	28	28	27
MIDE	22	23	23	23	21	23	25	24
USA	25	24	26	26	23	26	27	24
RUS+CAS	19	18	19	20	19	19	21	21
OCE	22	21	21	20	21	22	22	19
CAM	14	13	15	14	13	14	16	14
EU	11	11	11	11	11	12	12	11
CAN	8	9	8	8	7	9	8	8
Global	447	447	453	459	435	456	485	471

Table S3. Regional and global annual mean isoprene emission rates from 2013 to 2020 (unit: 10^{-10} kgC m^{-2} s^{-1}). Regional classification is seen in Fig. S5.

Isoprene 10^{-10} kgC m^{-2} s^{-1})	**2013**	**2014**	**2015**	**2016**	**2017**	**2018**	**2019**	**2020**
AMZ	2.9	3.1	3.3	3.1	3.0	2.9	3.1	3.2
SEAS	2.2	2.3	2.2	2.3	2.3	2.3	2.5	2.4
SAS	2.0	1.7	1.8	1.8	1.9	1.8	2.1	2.1
EQAF	2.0	1.9	1.9	2.0	1.9	2.0	2.1	2.1
CAM	1.6	1.6	1.8	1.7	1.6	1.7	1.9	1.7
RSAM	1.3	1.4	1.4	1.4	1.2	1.3	1.5	1.4
SAF	1.2	1.3	1.2	1.2	1.1	1.3	1.4	1.3
MIDE	1.1	1.2	1.2	1.2	1.1	1.2	1.3	1.2
CHN+KAJ	1.1	1.0	1.0	1.1	1.0	1.1	1.1	1.1
USA	1.0	1.0	1.1	1.1	0.9	1.1	1.1	1.0
NAF	0.8	0.8	0.8	0.8	0.8	0.8	0.9	0.9
OCE	0.9	0.8	0.8	0.8	0.8	0.9	0.9	0.8
EU	0.6	0.6	0.6	0.6	0.6	0.7	0.7	0.6
RUS+CAS	0.3	0.3	0.3	0.3	0.3	0.3	0.3	0.3
CAN	0.2	0.2	0.2	0.2	0.2	0.2	0.2	0.2
Global	1.1	1.1	1.1	1.1	1.0	1.1	1.2	1.1

References

Li, W., MacBean, N., Ciais, P., Defourny, P., Lamarche, C., Bontemps, S., Houghton, R. A., and Peng, S.: Gross and net land cover changes in the main plant functional types derived from the annual ESA CCI land cover maps (1992–2015), Earth Syst. Sci. Data, 10, 219-234, 10.5194/essd-10-219-2018, 2018.

Pu, J., Yan, K., Roy, S., Zhu, Z., Rautiainen, M., Knyazikhin, Y., and Myneni, R. B.: Sensor-independent LAI/FPAR CDR: reconstructing a global sensor-independent climate data record of MODIS and VIIRS LAI/FPAR from 2000 to 2022, Earth Syst. Sci. Data, 16, 15-34, 10.5194/essd-16-15-2024, 2024.